Optics Letters

High-power near-CW Raman lasing in mm-sized glass disks

D. C. Gold,[1,†] A. S. Bhadkamkar,[2,†] S. Carpenter,[1] L. T. Hogan,[3] M. Dwyer,[2] M. Beede,[1] R. H. Goldsmith,[3] D. van der Weide,[2] and D. D. Yavuz[1,*]

[1]Department of Physics, 1150 University Avenue, University of Wisconsin, Madison, Wisconsin, 53706, USA
[2]Department of Electrical and Computer Engineering, 1415 Engineering Drive, University of Wisconsin, Madison, Wisconsin, 53706, USA
[3]Department of Chemistry, 1101 University Avenue, University of Wisconsin, Madison, Wisconsin, 53706, USA
*Corresponding author: yavuz@wisc.edu
†These authors contributed equally to this work.

Received 26 May 2022; revised 15 July 2022; accepted 21 July 2022; posted 22 July 2022; published 9 August 2022

We experimentally demonstrate Raman lasing in a mm-sized CaF_2 disk, with an optical power output of the first Stokes sideband exceeding 100 mW in a near-continuous wave (CW) operation. The pump beam at a wavelength of 1.06 μm is coupled to the whispering gallery modes of the disk with the use of a tapered glass fiber. With the pump beam coupled to one of the resonator modes, we observe the generation of the first and the second Stokes sidebands at wavelengths of 1.1 μm and 1.14 μm, respectively. The conversion efficiency from the pump laser beam to the generated sidebands is ∼10%. These results open up the prospect of using such mm-sized disks as compact, highly efficient ultrafast modulators with modulation frequencies as high as 10 THz.

https://doi.org/10.1364/OL.465120

Over the last two decades, whispering gallery modes (WGM) of spherical or cylindrical glass resonators have found increasing use in nonlinear optics, photonics, and sensing [1–4]. WGMs can have very small volumes and high quality factors, making them ideal candidates for a variety of applications that require high laser intensity but low optical power. Furthermore, laser light can be coupled into WGMs using single-mode tapered fibers, resulting in highly compact [5] and mechanically stable devices [6]. For example, in these resonators, one can generate a broad discrete spectrum using the Kerr nonlinearity and produce a frequency-stabilized optical comb [7]. Temporal solitons can be formed in these systems that require very low optical pumping power [8]. Optical parametric oscillation using WGMs can be used to generate a broad spectrum in the mid-infrared [9]. The use of these resonators in efficient stimulated Raman scattering has also been explored [10–15]. Specifically, by using resonators with a size of ∼ 100 μm, CW Raman lasing of the Stokes beam can be achieved with pump power thresholds as low as ∼ 10 μW [10,11].

We have recently suggested the use of WGMs in glass resonators for producing highly efficient, compact optical modulators with modulation frequencies as high as 10 THz [16]. Here, the basic idea is that if sufficiently high pump and Stokes laser intensities are achieved inside the resonator, the crystal can be viewed as an ensemble of molecules coherently vibrating at the frequency of the Raman transition, $\omega_m = \omega_{pump} - \omega_{Stokes}$ [17–22]. Any other laser at a frequency ω can then be coupled to the resonator and will be frequency modulated, producing upshifted and downshifted sidebands at frequencies $\omega + \omega_m$ and $\omega - \omega_m$, respectively [23]. The frequency modulation is due to four-wave mixing nonlinearity enabled by the Raman interaction. This process, which we term molecular modulation, can happen in a variety of different physical platforms. For example, very recently, CW frequency upconversion from the mid-infrared to the visible from a few hundred molecules using an optomechanical nanocavity has been demonstrated [24]. Molecular modulation is predicted to be remarkably efficient in WGMs of glass resonators. Detailed numerical simulations show that such a device can achieve single-pass CW modulation efficiencies at the level of 10%, but would require pump power values as high as 1 W coupled to the resonator mode with intensities exceeding 100 MW/cm^2 [16].

In this Letter, we show progress toward such a device by extending the use of WGMs to the high-power CW pump laser regime and to relatively large mm-sized glass disks. Specifically, we use a CaF_2 disk with a radius of 6.5 mm, couple a pump laser beam at a wavelength of 1.06 μm to the WGMs of the disk, and study Raman lasing of the first and second Stokes sidebands. As we discuss below, we are able to couple pump light with optical powers exceeding 1 W to the disk. At our maximum coupled pump power, we have observed the generation of more than 140 mW in the first Stokes, and more than 3 mW in the second Stokes sidebands, respectively, in near-CW operation. As we discuss below, near-CW means that the pump laser is not locked to one of the resonator modes; rather, the pump frequency is slowly scanned through a WGM resonance. To the best of our knowledge, the power values in the generated Stokes sidebands are the highest-ever reported using these systems, more than an order of magnitude higher than what was achieved before [15]. The wavelengths of the produced first and second Stokes sidebands are 1.1 μm and 1.14 μm, respectively. The conversion efficiency from the pump laser beam to the generated sidebands is ∼ 10% and is reasonably high. These results open

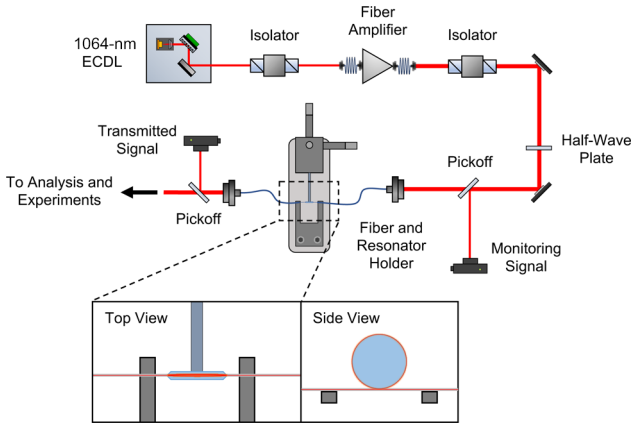

Fig. 1. Simplified schematic of the experiment. The pump laser system, an external cavity diode laser (ECDL) followed by a fiber amplifier, is coupled to a bare fiber, which is tapered to a diameter of approximately 2 μm at its center. The tapered section of the fiber is brought into close contact with a CaF_2 disk.

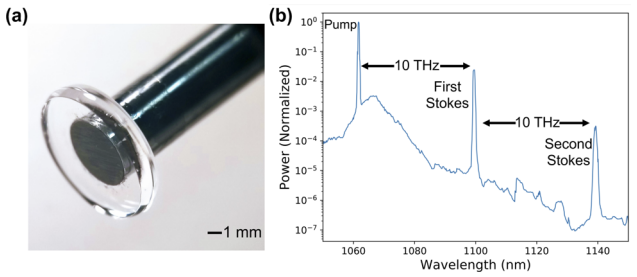

Fig. 2. (a) Photograph of the CaF_2 disk with a radius of 6.5 mm and a thickness of 2 mm. (b) Spectrum of the transmitted light through the tapered fiber when the frequency of the pump light is tuned close to one the WGMs of the disk and its transmitted power is increased to approximately 1 W. Through cascaded Raman lasing, the pump laser at 1.06 μm produces first and second Stokes sidebands at wavelengths of 1.1 μm and 1.14 μm, respectively.

up the prospect of using such mm-sized disks as compact, highly efficient ultrafast modulators with modulation frequencies as high as 10 THz.

At such high power values for the pump and Stokes laser beams, we observe shifts and broadening of the resonances due to thermal heating, as well as complicated temporal dynamics induced by Raman lasing. We find that the temporal dynamics of Raman lasing differ greatly depending on to which WGM mode of the disk that the pump light is coupled. For some modes, the generated Stokes laser pulse has a sharp initial spike followed by a plateau, while for others, both pump and Stokes pulses immediately approach a steady-state-like plateau. Due to these complications, we have not attempted to lock the frequency of the pump laser to one of the modes of the resonator. We have, instead, operated our device in a near-CW regime, where we scan the frequency of the pump laser over the WGM resonances, and produce the Raman sidebands over ∼1-ms time scales. The reported power values for the generated Stokes sidebands are measured over these ∼1-ms scans, and do not correspond to true CW operation.

Figure 1 shows the simplified schematic of the experiment. To produce the desired high-power pump laser beam, we start with an external cavity diode laser (ECDL) at a wavelength of 1.06 μm. The ECDL is custom built with an optical power of 20 mW and a free-running linewidth of approximately 0.5 MHz. The grating of the external cavity is placed on a piezoelectric transducer (PZT), which allows slight adjustments of the cavity length thereby tuning its frequency. The mode-hop free tuning range of the ECDL frequency is approximately 6 GHz. After passing through a Faraday isolator, the beam is amplified to a CW power value as high as 10 W with a ytterbium fiber amplifier. After further isolation and polarization control, the amplified beam is coupled to a bare single-mode fiber, which is tapered to a diameter of approximately 2 μm at its center. The tapered section of the fiber is brought into close contact to the CaF_2 disk using a 3D optomechanical stage. The pump light is coupled to the WGM disk resonances through evanescent mode coupling between the tapered fiber and the disk. The fiber is bi-tapered and provides both input and output coupling to the disk. After the fiber, the output is collimated and a small portion of the output is picked up with a photodiode to detect the overall transmitted pump signal. The rest of the output is sent to a custom-made grating spectrometer to measure its spectral content, as well as the generated power in the Stokes and second-Stokes sidebands.

CaF_2, being a crystalline material, has low scattering losses and its mechanical hardness enables nanometer surface polishing to reduce surface scattering. It is fairly resistant to water absorption and has a high Raman gain [10]. Due to these advantages, CaF_2 was chosen for this work. The fabrication of the glass resonators began with CaF_2 cylindrical disks of radius 6.5 mm and thickness of 2 mm. Initial grinding was performed using abrasive diamond films to create a wedge shape along the rim of the disk. The wedge shape is required to confine the modes, thereby decreasing the volume of the WGMs. The initial grinding was followed by polishing with diamond abrasive of successively decreasing grit size down to 50 nm. The final polished disk was glued to a steel rod, which helped with the mounting and integration of the resonator with the rest of the optical setup. A photograph of the disk attached to a steel rod is shown in Fig. 2(a).

The tapered fiber is fabricated using a mechanical fiber puller where the central region of the fiber is heated with a hydrogen flame. We have empirically found that fibers whose diameters at the taper are ∼ 2 μm perform best for the operation of the device. Fibers with diameters smaller than 2 μm are susceptible to optical damage due to the high power value of the pump, while larger diameter fibers do not produce sufficient evanescent wave coupling to the WGMs of the disk. The optical damage that we observe typically is complete fracture of the tapered section. While we do not completely understand the mechanism, we believe it is thermally initiated; likely a dust particle on the surface absorbs laser light and produces a thermal hot spot, initiating structural breakdown of the fiber.

We characterize the WGMs of the disk by scanning the frequency of the pump laser and looking at the dips of the transmitted signal at the fiber output. When the frequency of the pump laser beam is brought into resonance with one of the WGMs of the disk and its power through the fiber is increased to higher than 300 mW, we observe the generation of the first and second-Stokes sidebands at wavelengths of 1.1 μm and 1.14 μm, respectively. A sample wavelength scan of the output obtained with the grating spectrometer, which clearly shows the pump, the first-Stokes, and second-Stokes sidebands, is shown in Fig. 2(b).

Figure 3 shows the transmitted power of the pump through the fiber as its frequency is scanned through the WGM resonances.

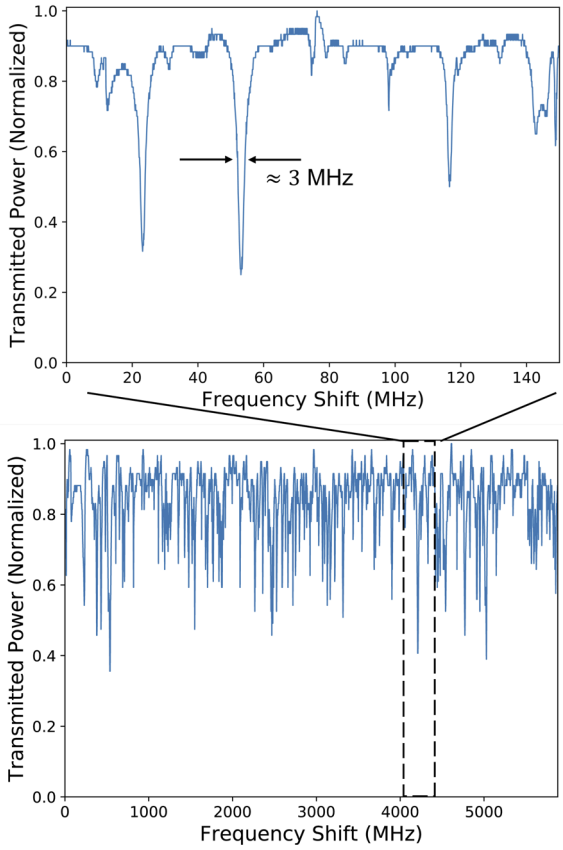

Fig. 3. Transmission of the pump laser beam through the tapered fiber as its frequency is scanned over 6 GHz. The inset shows pump transmission over a narrower frequency range of 150 MHz. We typically observe the width of the resonances to be approximately 3 MHz, which puts the quality factor of the WGMs at $Q \sim 5 \times 10^7$.

The free spectral range (FSR) of the resonator is 7.3 GHz, so the main scan, which is over 6 GHz, is approximately 80% of the FSR. We are not able to scan over many FSRs due to the mode-hop free tuning-range limitation of the ECDL. We observe coupling to many WGMs, with the depth of the transmission dips to be as large as 70% for some of the modes. This indicates reasonably good evanescent mode coupling between the tapered fiber and the disk. The inset in Fig. 3 shows the transmission of the pump laser through the fiber over a much narrower frequency scan of 150 MHz. We observe the width of most of the resonances to be ~ 3 MHz, which puts the quality factor of the disk at a value of $Q \sim 5 \times 10^7$. The data shown in Fig. 3 and the reported Q value are obtained at a low power of <1 mW for the pump laser beam. As the pump power is increased to 1 W, the loaded-Q value drops substantially, as much as an order of magnitude for some of the WGM resonances.

When the optical power of the pump laser is increased, we observe Raman lasing as the frequency of the pump is tuned to the WGMs of the disk. We find that coupling to some of the modes results in efficient Raman lasing, while other modes may not produce lasing at all. This is likely due to the different mode volumes of the WGMs, resulting in significantly different circulating pump laser intensity. Figure 4 shows the generated optical power in the first Stokes and second Stokes sidebands as the optical power in the pump laser beam is increased. Reaching the Raman lasing threshold requires 100 to 150 mW of pump

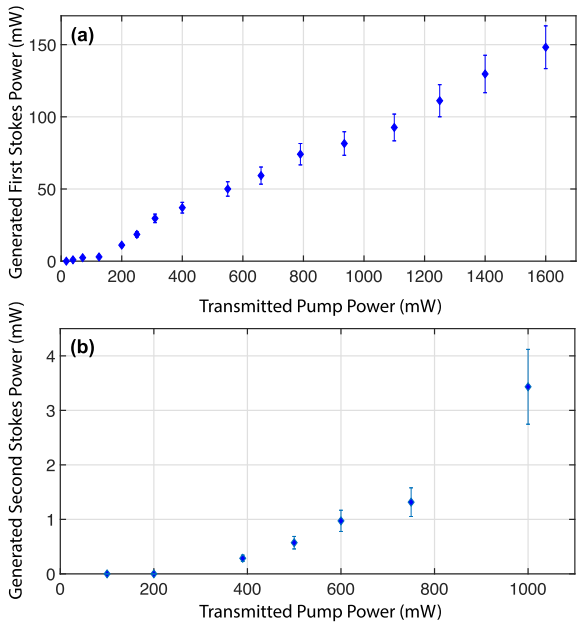

Fig. 4. Optical power generated in (a) the first Stokes and (b) the second Stokes sidebands as the pump power transmitted through the tapered fiber is varied. At our highest pump power values, we produce a first Stokes power exceeding 140 mW and second Stokes power exceeding 3 mW.

power. At our highest pump power, we produce a first Stokes power exceeding 140 mW. The optical power in the second Stokes sideband exceeds 3 mW. To the best of our knowledge, these power values are the highest ever reported in these systems using near-CW operation. The power values that are reported in Fig. 4 are for the WGM mode (or a couple of modes) that produces the most efficient Raman lasing. In addition to this mode with the highest Raman lasing output, we typically observe that within an FSR, there are ~ 10 modes of the resonator that produce a first Stokes power a factor of 5 to 10 lower than what is reported in Fig. 4.

The observed Raman lasing threshold of Fig. 4 (~ 100 mW) is within an order of magnitude of the calculated threshold, based on the known Raman gain coefficient, observed Q-value of the resonator, and the calculated mode volume for the pump laser beam [10,11]. The discrepancy between the calculation and the experimental observation is likely due to the imperfect mode overlap between the pump and Stokes modes.

Our detailed numerical simulations of this system, which includes solving coupled Maxwell's and density matrix equations numerically, are reported in Refs. [16] and [25]. As of yet, we have not been able to obtain good quantitative agreement between our numerical simulations and experimental results reported here. This is likely due to the high circulating intensities in the disk, resulting in substantial thermal effects, and also to the presence of competing nonlinear optical processes. For example, at high values of the coupled pump power, we have observed significant broadening of the spectrum near the pump laser wavelength due to Kerr self-phase modulation. This broadening is approximately 20 nm wide and shows as a broad shoulder around the pump peak, which can be seen in the output spectrum of Fig. 2(b) (near the pump wavelength of 1.06 μm). We also observe substantial green fluorescence from the disk, which is likely due to two-photon absorption from the pump

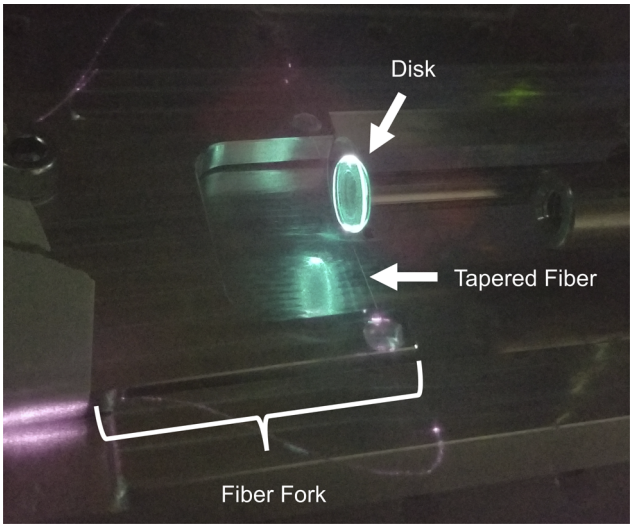

Fig. 5. Photograph of the disk fluorescing in the green, which is likely due to two-photon absorption from the pump laser beam. This fluorescence is a clear indication of the presence of competing nonlinear optical processes in the disk.

laser. A photograph of the crystal fluorescing in the green when the lab is dark is shown in Fig. 5.

In conclusion, we have studied high-power Raman lasing in mm-sized glass disks with the highest power outputs reported to date in the generated Stokes sidebands in near-CW operation. In future work, we plan to extend our numerical simulations to include the effects of competing nonlinear optical processes in addition to Raman lasing. With such an extension, it may be possible to predict the observed Raman lasing output of the first and second Stokes sidebands, which are reported in Fig. 4. Future experimental work will include detecting the generated anti-Stokes sidebands as well as introducing a separate laser beam to the setup and investigating its modulation due to the intense circulating pump and Stokes intensities inside the resonator.

Funding. University of Wisconsin-Madison (Research Forward 1).

Acknowledgments. We thank Josh Karpel for many helpful discussions and for his contributions at the early stages of this project. We also would like to thank Andy Bean from PIKE Technologies for his help in characterizing the surface of the glass disks. Support for this research was provided by the University of Wisconsin—Madison Office of the Vice Chancellor for Research and Graduate Education with funding from the Wisconsin Alumni Research Foundation.

Disclosures. The authors declare no conflicts of interest.

Data availability. Data underlying the results presented in this paper are not publicly available at this time but may be obtained from the authors upon reasonable request.

REFERENCES

1. A. B. Matsko and V. S. Ilchenko, IEEE J. Sel. Top. Quantum Electron. **12**, 3 (2006).
2. V. S. Ilchenko and A. B. Matsko, IEEE J. Sel. Top. Quantum Electron. **12**, 15 (2006).
3. G. C. Righini, Y. Dumeige, P. Féron, M. Ferrari, G. N. Conti, D. Ristic, and S. Soria, Riv. Nuovo Cim. **34**, 435 (2011).
4. K. D. Heylman, K. A. Knapper, E. H. Horak, M. T. Rea, S. K. Vanga, and R. H. Goldsmith, Adv. Mater. **29**, 1700037 (2017).
5. B. Min, T. J. Kippenberg, and K. J. Vahala, Opt. Lett. **28**, 1507 (2003).
6. Y. L. Li and P. F. Barker, Sensors **18**, 4184 (2018).
7. P. Del'Haye, O. Arcizet, A. Schliesser, R. Holzwarth, and T. J. Kippenberg, Phys. Rev. Lett. **101**, 053903 (2008).
8. T. Herr, V. Brasch, J. D. Jost, C. Y. Wang, N. M. Kondratiev, M. L. Gorodetsky, and T. J. Kippenberg, Nat. Photonics **8**, 145 (2014).
9. Q. Sun, W. Wu, Y. Wang, Y. Yang, L. Shi, X. Ming, L. Wang, K. Wang, W. Zhao, and W. Zhang, Nanotechnology **33**, 210003 (2022).
10. I. S. Grudinin and L. Maleki, Opt. Lett. **32**, 166 (2007).
11. I. S. Grudinin and S. Maleki, J. Opt. Soc. Am. B **25**, 594 (2008).
12. S. M. Spillane, T. J. Kippenberg, and K. J. Vahala, Nature **415**, 621 (2002).
13. T. Kato, A. Hori, R. Suzuki, S. Fujii, T. Kobatake, and T. Tanabe, Opt. Express **25**, 857 (2017).
14. T. J. Kippenberg, S. M. Spillane, B. Min, and K. J. Vahala, IEEE J. Sel. Top. Quantum Electron. **10**, 1219 (2004).
15. P. Latawiec, V. Venkataraman, A. Shams-Ansari, M. Markham, and M. Loncar, Opt. Lett. **43**, 318 (2018).
16. J. T. Karpel, D. C. Gold, and D. D. Yavuz, Opt. Express **27**, 34154 (2019).
17. S. E. Harris and A. V. Sokolov, Phys. Rev. Lett. **81**, 2894 (1998).
18. A. V. Sokolov, D. R. Walker, D. D. Yavuz, G. Y. Yin, and S. E. Harris, Phys. Rev. Lett. **85**, 562 (2000).
19. J. Q. Liang, F. L. Kien, and K. Hakuta, Phys. Rev. Lett. **85**, 2474 (2000).
20. K. Ihara, C. Eshima, S. I. Zaitsu, S. Kamitomo, K. Shinzen, Y. Hirakawa, and T. Imasaka, Appl. Phys. Lett. **88**, 074101 (2006).
21. J. K. Brasseur, K. S. Repasky, and J. L. Carlsten, Opt. Lett. **23**, 367 (1998).
22. H. S. Chan, Z. M. Hsieh, W. H. Liang, A. H. Kung, C. K. Lee, C. J. Lai, R. P. Pan, and L. H. Peng, Science **331**, 1165 (2011).
23. D. C. Gold, J. T. Karpel, E. A. Mueller, and D. D. Yavuz, Opt. Lett. **43**, 1003 (2018).
24. W. Chen, W. Chen, P. Roelli, H. Hu, S. Verlekar, S. P. Amirtharaj, A. I. Barreda, T. J. Kippenberg, M. Kovylina, E. Verhagen, A. Martínez, and C. Galland, Science **374**, 1264 (2021).
25. J. T. Karpel, "Numerical simulation of intense ultrafast quantum phenomena," (University of Wisconsin-Madison, 2019).